Experiments in Fluids 23 (1997) 281–287 © Springer-Verlag 1997

LIF-LII measurements in a turbulent gas-jet flame

R. L. Vander Wal

Abstract Detection of soot by laser-induced incandescence (LII) and fuel-rich (PAH containing) regions by laser-induced fluorescence (LIF) is demonstrated in a turbulent, $Re = 2500$, ethylene gas-jet diffusion flame. Simultaneous combined LIF–LII images allow identification of regions containing PAH or soot and their relative spatial relationship. Separate LII images confirm the identity of the soot containing regions shown in the LIF–LII images. Variations in the size, structure, spatial location and intensity of the PAH and soot containing regions are shown qualitatively in the images and quantified through histograms of image intensities and spatial extents.

1 Introduction

Significant pyrolysis within fuel-rich regions prior to oxidizer entrainment leads to PAH and soot which are more difficult to oxidize and creates the potential for emission of unburnt fuel products in a range of practical combustion processes (Longwell 1984). To provide a fundamental understanding of fuel/air mixing and burning in practical combustion processes, laboratory studies have focused on turbulent diffusion flames as model systems. Ionization (Lockwood and Odidi 1975), chemical (Nishida and Mukora 1982), and optical probes (Copalle and Joyeux 1994), absorption followed by tomographic techniques (Nyden et al. 1996), laser-induced fluorescence (Tait and Greenhalgh 1994), and laser-light scattering (Dasch and Heffelfinger 1991; Miake-Lye and Toner 1987; Turns et al. 1989; Lysaght et al. 1982; Chen and Roquemore 1986) have revealed various aspects of the structure of turbulent diffusion flames. One- and two-dimensional laser light scattering studies were particularly useful in revealing the soot distribution within soot containing turbulent diffusion flames (Dasch and Heffelfinger 1991; Miake-Lye and Toner 1987; Turns et al. 1989). In each of these laser-light scattering studies from soot, large soot-free pockets were observed throughout a range of axial heights. These regions are often enveloped by soot containing regions and soot streaks.

A prime motivation of the soot scattering investigations was to visualize soot zones as markers for the flame front (Miake-Lye and Toner 1987; Turns et al. 1989). Instantaneous planar visualization of flame front locations within turbulent diffusion flames can provide data to test flamelet models of turbulent flames by serving as a surrogate indicator of the flame front location and measure of flame surface area (Turns et al. 1989). Spatial location of the fuel-rich regions in relation to the soot containing regions would also aid modelling studies of soot formation coupled with radiation within turbulent diffusion flames (Young and Moss 1995). In the turbulent diffusion flames studied by light scattering, the fuel/air ratio on either side of the soot containing regions remains unidentified and could correspond to either fuel-rich or fuel-lean regions (Prado et al. 1976). Unambiguous location of the flame front location and curvature requires knowledge of the fuel-rich side of the soot zone thereby locating the flame as opposite of the fuel-rich region.

To locate fuel-rich and soot containing regions within a model turbulent flame, simultaneous laser-induced fluorescence (LIF) and laser-induced incandescence (LII) (denoted as LIF–LII images) images were collected. LII has been widely demonstrated for the detection of soot within diffusion flames (Vander Wal and Weiland 1994; Quay et al. 1994; Vander Wal and Dietrich 1995; Ni et al. 1995; Shaddix et al. 1995; Cignoli et al. 1994; Vander Wal et al. 1996a, b; Vander Wal 1996a, b, c). Compared to scattering, LII should yield a superior measure of the soot concentration and distribution since the signal is proportional to soot volume fraction (Melton 1984; Hofeldt 1993). LIF within fuel-rich regions of diffusion flames is considered to arise from PAHs (Smyth et al. 1985; Gomez et al. 1987; Vander Wal et al. 1996b; Vander Wal 1996b, c). Conversely, fuel-lean regions do not contain PAHs due to the lack of reactants and likely concurrent oxidation processes.

Recently simultaneous LIF and LII images have been obtained within laminar diffusion flames successfully revealing both fuel-pyrolysis (PAH containing) and soot containing regions along flow streamlines (Vander Wal et al. 1996b; Vander Wal 1996b, c). Since simultaneous LIF–LII images may be obtained using a single laser-shot, the combined fluorescence/incandescence imaging technique is ideally suited for time-varying asymmetric combustion processes such as turbulent flames. To clearly distinguish the soot and PAH containing regions revealed by the LIF–LII images, separate but equivalent (separate in time, identical in spatial location) LII images

Received: 9 September 1996/Accepted: 4 February 1997

R. L. Vander Wal
Nyma@NASA-Lewis
M.S. 110-3
21,000 Brookpark Rd.
Cleveland, OH 44135

RVW gratefully acknowledges support under NASA contract NAS3-27186 and aid of Mr. Kirk A. Jensen with some of the experiments and data analysis.

were also obtained. Histogram analysis of the LIF–LII and LII images quantify the spatial distributions of the PAH/soot in both formation and oxidation processes at different axial heights within the flame.

2 Experimental

The experimental configuration is similar to previous measurements (Vander Wal et al. 1996a, b). Light at either 1064 or 266 nm was used for LII and combined LIF–LII measurements respectively. An 8× Galilean telescope of spherical UV fused silica lenses followed by a pair of positive spherical cylindrical lenses and an aperture formed the 266 nm light into a 50 mm high laser sheet. An 8× Galilean telescope followed by a 1500 mm spherical cylindrical lens formed the 1064 nm light into a laser sheet. Each laser sheet passed through the jet centerline. Based on pulsewidths of 10 and 5 ns for the 1064 and 266 nm light, estimated laser sheet intensities were 7×10^7 and 8×10^6 W/cm^2 respectively. Due to varying soot loading in the annular region, the calculated laser intensities must be considered an upper bound for the laser intensity at the jet centerline.

Previous measurements of the LII signal dependence upon excitation laser intensity have shown an initial steeply rising portion followed by a "plateau" region (Vander Wal and Weiland 1994; Ni et al. 1995). In this region, the LII signal is rather independent of the precise value of the laser intensity. Additionally, typical laser shot-to-shot energy fluctuations are small relative to the absolute laser energy in this regime. Experiments reported here using 1064 nm light as the excitation wavelength were performed in this intensity range. Those performed using 266 nm light to excite incandescence were near the onset of this range. Prior experiments have also shown that the fluorescence is saturated at these laser intensities

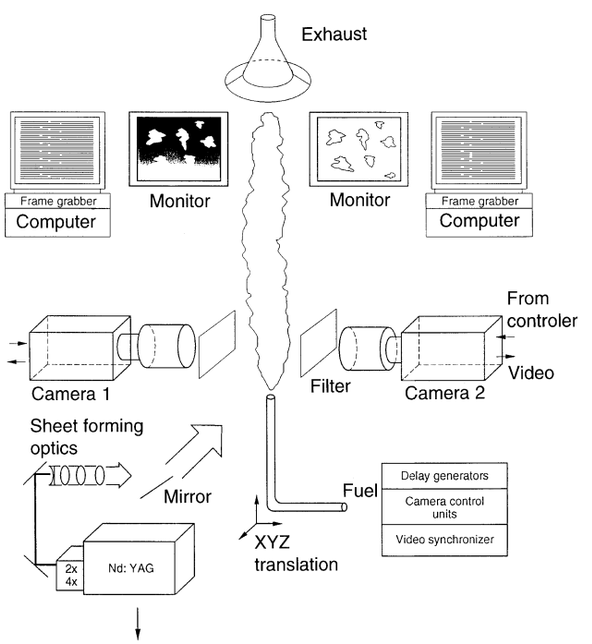

Fig. 1. Experimental diagram

(Vander Wal et al. 1996b; Vander Wal 1996b). Decreasing the 266 nm excitation intensity by $\frac{1}{3}$ resulted in less than a 10% decrease in the LIF signal level. Thus the simultaneous LIF–LII and separate LII images were not normalized for laser sheet intensity variations.

Opposing gated intensified cameras fitted with ultraviolet f4.5/105 mm (adjustable) focal length camera lenses and 40 mm extension tubes captured the LII (using 1064 nm excitation) and simultaneous LIF–LII images (using 266 nm excitation). The object magnification yielded a pixel resolution of 27 pixels per millimeter. The actual spatial resolution, determined by using a replica of the 1951 Air Force imaging standard was found to be approximately 70 μm. Bandpass interference filters transmitting 400–450 nm preceded the gated intensified array cameras. Frame-grabbers digitized the images for transfer to the host computer. Delay generators controlled the relative timing of the camera video signals, the firing of the laser and camera detection gates. The delay between the 266 and 1064 nm excitation pulses was 1100 ns thereby yielding essentially simultaneous LIF–LII and separate LII images. The ethylene flow rate through the 1 mm inner diameter vertically oriented stainless tube was 3.0 slm resulting in a lifted flame and cold flow Reynolds number of 7500. The approximate visible flame length was 30 cm.

3 Simultaneous paired LIF–LII images

3.1 LIF and LII signal interpretation

Light at 1064 nm has been demonstrated to excite incandescence while not creating photochemical interferences or exciting fluorescence (Vander Wal and Weiland 1984; Vander Wal et al. 1996a, b; Vander Wal 1996b). Spectrally resolved emission scans of the laser-induced signal (fluorescence/incandescence) using 266 nm light have similarly indicated an absence of photochemical interferences within the fuel-rich region of laminar ethylene diffusion flames (Vander Wal et al. 1996b; Vander Wal 1996b). Although interferences can arise within soot containing regions (Bengtsson and Alden 1991; Beretta et al. 1992) other investigators have found these interferences to provide an accurate surrogate measure of the soot concentration (Bengtsson and Alden 1995). In the experiments by Bengtsson and Alden, laser excited fluorescence from vaporized C_2 molecules (from the laser-heated soot) was used as a measure of the soot concentration. The excitation wavelengths used in the present study, 1064 and 266 nm, do not coincide with any resonant electronic transitions of potential vaporized species from soot such as carbon atoms, C_2 and C_3 molecules. Thus images obtained using 266 nm excitation should accurately reveal both soot and PAH containing regions.

With laser intensities greater than 5×10^6 W/cm^2 at 266 nm, the incandescence from typical soot concentrations within these laminar flames has appeared more intense (roughly 2–3×) than the PAH fluorescence thus serving to distinguish PAH and soot containing regions (Vander Wal et al. 1996b; Vander Wal 1996b, c). These observations agree with expectations that molecular fluorescence would saturate at far lower laser intensities than laser-induced incandescence (Eckbreth

1988). LII has been widely recognized as presenting overwhelming signals to other optical diagnostics such as CARs (Eckbreth et al. 1986). Alternatively, the PAH and soot containing regions shown in the LIF–LII images may be differentiated by comparison to separate LII images as demonstrated here.

In principle, complimentary experiments to detect the PAHs by using laser intensities insufficient to cause incandescence would more clearly distinguish PAH from soot containing regions. In practice, insufficient PAH fluorescence signal intensity was attainable at laser intensities that did not result in incandescence from soot. Hence higher laser intensities were used to produce simultaneous LIF–LII images to illustrate by comparison with separate but temporally coincident LII images the PAH containing regions within the turbulent flame. With the fastest measured turbulent velocities on the order of 10 m/s, in the 1.1 μs separation between the 266 and 1064 nm light pulses, the flow may be considered stationary. Additionally, this time separation allows the LII excited by the 266 nm light to decay prior to detecting the LII excited by the subsequent 1064 nm light pulse.

3.2
Image results

Figures 2–4 show simultaneous LIF–LII images obtained by using 266 nm excitation and nearly temporally coincident LII images obtained using 1064 nm excitation. Representative images were selected at each of the three heights. The three LIF–LII and corresponding but separate LII image pairs are temporally uncorrelated within each figure. The lower height of the images shown in Figs. 2–4 begin at 7.6, 13.1 and 18.6 cm above the burner. In each figure, the LIF–LII images are shown in the left column while the LII images appear in the right column. The LII images reveal soot incandescence while the LIF–LII images contain both incandescence from soot and fluorescence from PAHs. Comparison of the LIF–LII images with the corresponding LII images distinguishes the fluorescence from the incandescence.

As observed in the LII images in Figs. 2b, d and f, low in the flame the soot containing regions appear as elongated narrow streaks often oriented vertically. Both small and large scale vortex motions are indicated by the size variation of the curved soot streaks. As shown in Figs. 2a, c and e, PAH regions, revealed by fluorescence, generally appear near the jet axis while soot containing regions, revealed by incandescence, generally appear away from the jet axis. While soot often borders the fluorescing regions, both soot and PAH regions border dark regions (nonfluorescing and nonincandescing).

Comparison of the simultaneous LIF–LII and LII images in Fig. 3 higher in the flame reveals soot containing regions which are significantly larger in spatial extent, appearing both as streaks and pockets compared to the lower axial height. Similar to Fig. 2, the PAH containing regions are located nearer the jet centerline while soot containing regions are located along the outer periphery of the flow. There also is an absence of "dark"

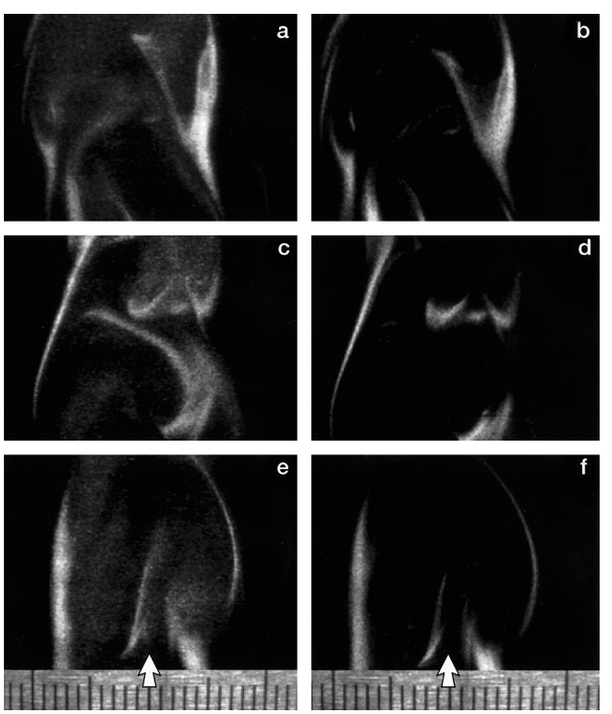

Fig. 2a–f. Simultaneous LIF–LII images (**a**, **c**, **e**) obtained using 266 nm excitation and separate LII images (**b**, **d**, **f**) obtained using 1064 nm excitation. The extent of each image is from 7.6 to 9.5 cm above the burner. The spatial scale is in millimeters. The white arrow locates the jet centerline axis for each column of images

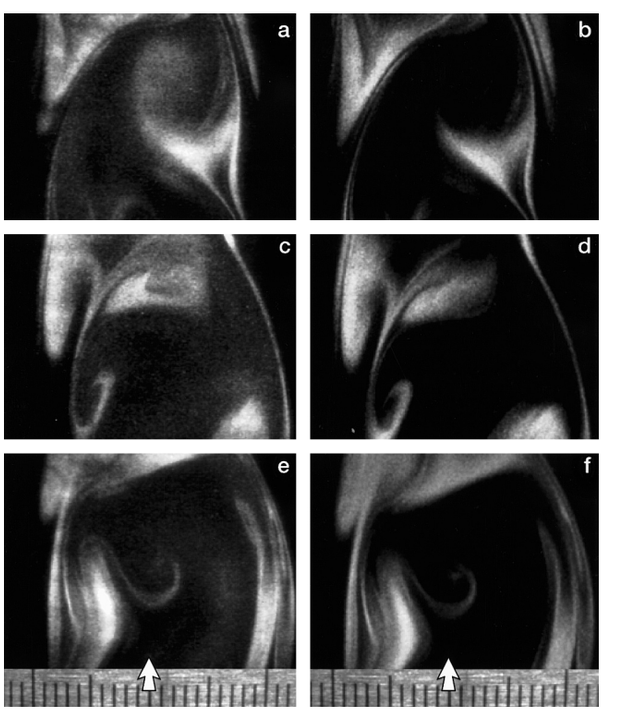

Fig. 3a–f. Simultaneous LIF–LII images (**a**, **c**, **e**) obtained using 266 nm excitation and separate LII images (**b**, **d**, **f**) obtained using 1064 nm excitation. The extent of each image is 13.1 to 15.0 cm above the burner. The spatial scale is in millimeters. The white arrow locates the jet centerline axis for each column of images

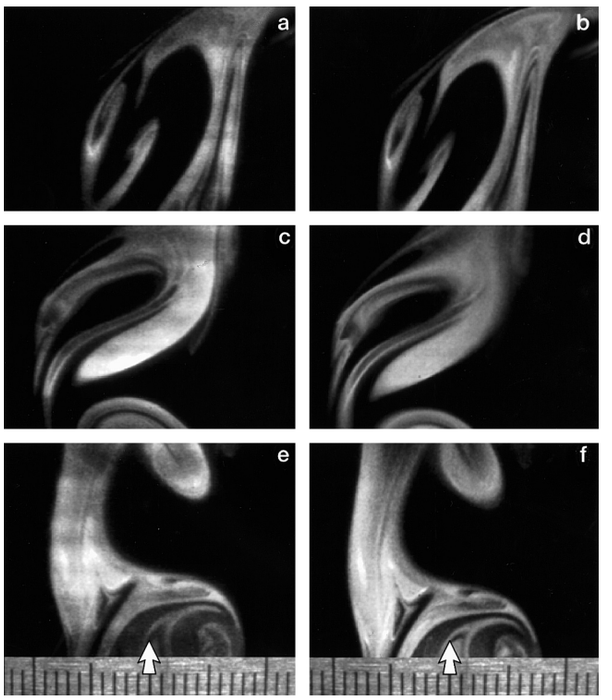

Fig. 4a–f. Simultaneous LIF–LII images (**a**, **c**, **e**) obtained using 266 nm excitation and separate LII images (**b**, **d**, **f**) obtained using 1064 nm excitation. The extent of each image is 18.6 to 20.5 cm above the burner. The spatial scale is in millimeters. The white arrow locates the jet centerline axis for each column of images

or nonfluorescing regions in the instantaneous LIF–LII images at this height.

At the highest axial height shown in Fig. 4 no PAH fluorescence is observed by comparison of the LIF–LII and LII images. Soot structures are largely connected and generally are located along the jet centerline. Regions of low intensity in the LIF–LII images which often corresponded to fluorescence now represent low soot concentrations as seen by comparison with the separate LII images.

3.3
Image discussion

The thin soot streaks of low soot and PAH concentrations at the lowest axial height is consistent with soot formation processes being in the earliest stages. Since the PAH producing and soot formation reactions require a finite temperature–time product, their appearance indicates that a minimum threshold in temperature–time has been achieved. At this lowest axial height, little time at elevated temperature has elapsed for fuel pyrolysis and soot formation/growth reactions to occur.

With increasing integrated temperature–time, soot formation/growth continues resulting in the increased soot concentration at higher axial heights as seen in Fig. 3. Similarly, PAH formation/growth also continues with increasing integrated temperature–time resulting in higher PAH concentrations in the fuel-rich regions. That the dark regions near the jet axis seen in Fig. 2 correspond to fuel-rich regions of unpyrolyzed fuel is suggested by the absence of such regions at higher axial heights as in Fig. 3. If turbulence had caused air-entrainment resulting in these dark regions being fuel-lean, then persistence of these regions and additional air-entrainment would be expected to be observed at the higher axial height shown in Fig. 3 as well. Thus the non-fluorescing and non-incandescing regions near the jet axis seen in Fig. 2 likely have not yet reached the minimum threshold in temperature–time.

At the highest axial height illustrated by Fig. 4, depletion of PAHs through both soot growth processes and oxidation likely account for the absence of PAHs. Turbulence acts to both break up fuel-rich regions and entrain oxidizer into the fuel-rich regions. Since molecular oxidation proceeds at far faster rates than soot oxidation, it is not surprising to find large regions of unoxidized soot yet no PAHs as seen by the high similarity between the LIF–LII and LII images. Because PAHs are likely to oxidize last among molecular fuel pyrolysis products due to their high thermal stability, at large axial heights any enclosed regions bounded by soot are likely to be fuel lean as demonstrated by the absence of fluorescence in the LIF–LII images.

Typically fuel-rich regions within both laboratory flames and practical combustion devices are visualized by laser-induced fluorescence of a fuel tracer such as acetone or acetaldehyde (Lozano et al. 1992; Arnold et al. 1990). The spatial extent of the fluorescence will provide a measure of both the extent of mixing and the flame position relative to the unburnt reactants. Often significant concentrations of the fluorescing additive are required. Not only does the fluorescence intensity vary with temperature (Suntz et al. 1991) but the fuel tracer pyrolyzes at temperatures well below those at the flame (Arnold et al. 1990). Unlike these other popular fuel tracers PAHs survive at high temperatures without undergoing fragmentation by virtue of resonance stabilization (Stein and Fahr 1985). Moreover PAHs arise as natural fuel pyrolysis products and so serve as natural fuel tracer species in soot forming flames. The first appearance of PAHs within a flame identifies gas volume elements that have experienced sufficient temperature–time histories to produce PAHs. Conversely, the absence of PAH fluorescence in the images obtained using 1064 nm excitation highlights the ability of LII to detect only solid carbonaceous soot apart from fuel pyrolysis products when using long wavelength excitation.

3.4
Image statistical analysis

The image statistics presented here are intended to illustrate the statistical trends in the soot concentrations and spatial extent of PAH versus soot containing regions. Although the means of the distribution converged rapidly, the shape of the distributions (as judged by the distribution moments) did not. Some distributions exhibit asymmetry with some sharp transitions between adjacent bin intervals as shown below. While this can be partially attributed to the binning, because there is no apriori reason to expect such characteristics, these features suggest that a statistically converged sample has not yet been achieved. The purpose of the histograms was to illustrate methodology for extracting quantifiable information regarding the extent of fuel pyrolysis and/or soot distribution (spatial and concentration). As the introduction indicates,

such information is likely to be the type of experimental data that can be compared with modelling calculations of soot formation within turbulent diffusion flames.

In a laser-induced image, two quantities are readily defined. The white count (WC) is calculated here as the summed intensity of all pixels composing the image. A count of all pixels containing a nonzero value may be defined as the number (N). From a series of such images, a histogram of each quantity can be compiled. As each histogram represents a statistical distribution of the quantity of interest, both the average and width of the distribution are of interest.

While the N histograms provide a measure of the spatial extent of the quantity, the WC histograms provide a measure of the intensity. In the LII images, the WC histograms are proportional to the spatially integrated soot concentration. Comparison between the N histograms of the LIF–LII and separate LII images reveals the spatial extent of the PAH containing regions relative to those containing soot. While comparison between histograms computed from temporally equivalent LIF–LII and LII images would be most instructive, equipment and data storage limitations dictated that the histograms be obtained from temporally uncorrelated LIF and LII images obtained separately.

Figures 5a–c shows the WC histograms computed from a series of 210 individual LII images obtained at each axial height. For ease of presentation, each histogram has been equally scaled along the abscissa. The average value of the distribution provides a relative value of the soot concentration over each spatial location while the width provides a measure of the fluctuation. The distribution mean is indicated in each figure. As is suggested by the LII images of Figs. 2–4, the soot concentration increases with increasing axial height since soot formation/growth times increase with increasing axial position. This is verified by the mean value of the histogram intensity distributions shifting towards ever larger values with increasing axial height. The low average value in Fig. 5c reflects the onset of soot formation with many images containing very little soot. The conclusion of soot formation prior to significant oxidation is signalled by the average of the distribution shown in Fig. 5a, corresponding to the highest axial position, being the largest among the three heights studied.

While no particular functional form is expected for the distributions, the width of each distribution offers a measure of the fluctuation in the spatially integrated soot concentration within each imaged section of the flame. At the lowest axial height, the narrow distribution illustrated in Fig. 5c likely arises from intermittency in the soot formation reactions caused by turbulent fluctuations. The inset in Fig. 5c shows the distribution expanded 10 ×. The asymmetry in the distribution seen on this expanded scale again reflects the high probability of many images containing very little soot. At the highest axial height, both flame motion and varying amounts of air entrainment due to turbulent mixing likely control the distribution width. The narrow and highly peaked soot distribution in the central region of the flame indicates that fluctuation in the spatially integrated soot concentration is least across this section of the flame. Possible roughly comparable rates of soot formation/growth and oxidation may account for the relative lack of fluctuation. Variations in the

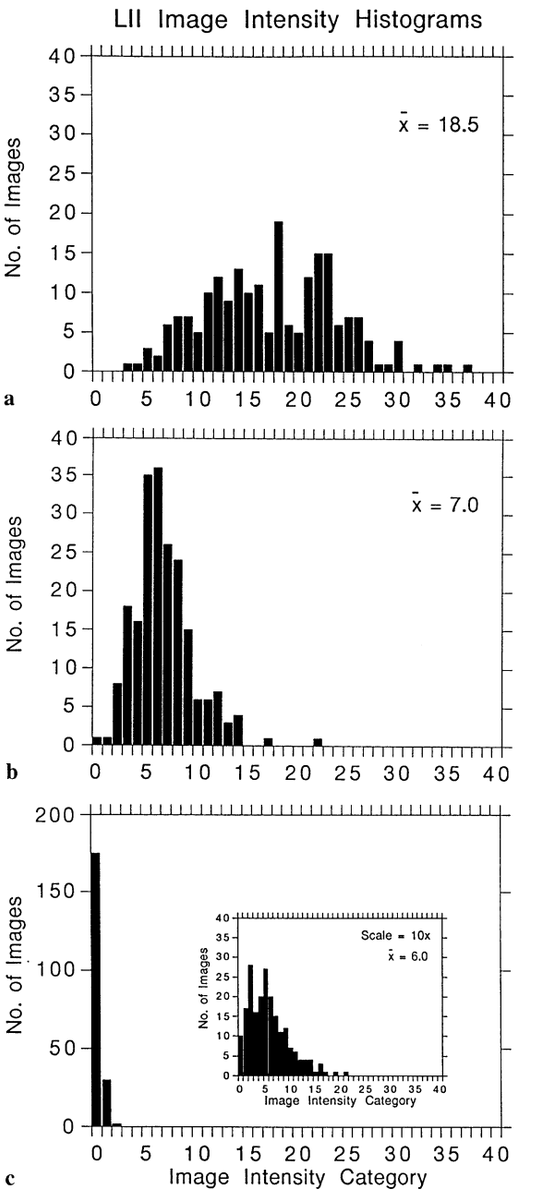

Fig. 5a–c. Histograms of the white count (WC) of pixel intensity from 210 temporally uncorrelated LII images at the axial positions corresponding to Figs. 2–4. **a** Panel corresponds to image data 18.6–20.5 cm above the burner (illustrated by Fig. 4); **b** panel corresponds to image data 13.1–15.0 cm above the burner (illustrated by Fig. 3); **c** panel corresponds to image data 7.6–9.5 cm burner (illustrated by Fig. 2)

LIF quantum yield with temperature prevent similar comparison of the LIF intensities.

Figures 6a–c show a comparison between the N histograms of the LIF–LII and separate LII images at each axial position studied. For ease of presentation, each histogram has been equally scaled along the abscissa. Each histogram was calculated from 210 images. The histogram corresponding to the LIF–LII images reflects both PAH and soot containing regions while that from the LII images reflects only the soot containing

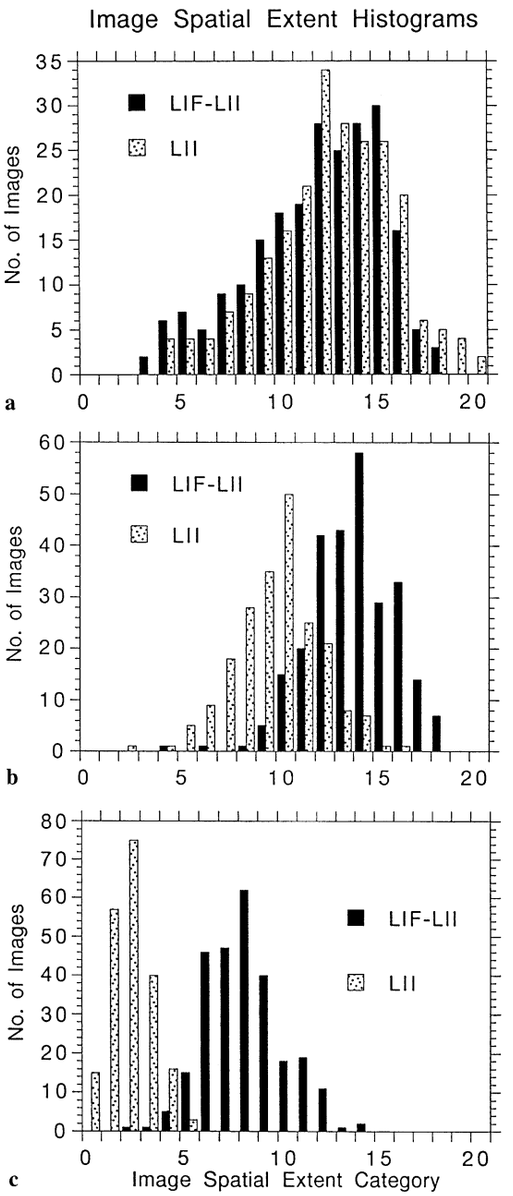

Fig. 6a–c. Histograms of the number (N) of pixels containing nonzero values from 210 temporally uncorrelated LIF–LII and separate LII images at the axial positions corresponding to Figs. 2–4. **a** Panel corresponds to image data 18.6–20.5 cm above the burner (illustrated by Fig. 4); **b** panel corresponds to image data 13.1–15.0 cm above the burner (illustrated by Fig. 3); **c** panel corresponds to image data 7.6–9.5 cm burner (illustrated by Fig. 2). Multiply each category by 19.1 to find the spatial coverage of each quantity in square millimeters

regions. As shown by comparison between the LIF–LII and LII histograms at the lowest indicated axial height illustrated in Fig. 6c, both the distribution width and mean value of the LIF–LII images is greater than those of the LII images reflecting both the significant amount of PAH present and variability in their formation due to turbulence. The difference between the histograms indicates the relative spatial extent of the PAH relative to the soot containing regions. Since many images did not contain detectable soot many of the "LII" images were blank and thus did not contribute to the LII histogram. As both PAH and soot formation/growth reactions continue, both the LIF–LII and LII N distributions reflect the increased amount of each species as measured by spatial extent. This is readily observed by comparison of the distributions in Fig. 6b (the intermediate axial height) to those in Fig. 6c (the lowest axial height). At this axial height, the PAH regions still comprise a larger spatial extent than the soot regions. At the highest axial height, the close correspondence between the two histograms shown in Fig. 6a indicates that PAH regions are absent. This is attributed to PAH oxidation preceding soot burnout.

5
Conclusions

PAH regions of the flame may be visualized via LIF. Soot containing regions may be located by the higher intensity level of the incandescence signal or, as demonstrated here, by comparison of simultaneous LIF–LII and separate LII images. Since the LIF–LII image may be obtained with a single laser shot, the combined fluorescence/incandescence technique is widely applicable to transient asymmetric combustion processes. Variations in the size, structure, spatial location and intensity of PAH and soot regions are visualized via LIF–LII and separate LII images. Defining fuel-rich regions locates the flame front and curvature by spatially establishing the fuel-rich side of the soot streaks and regions. Statistical analysis using histograms of the LII images quantifies the variation in soot concentration with axial height and the fluctuation at each height. Comparison of the LIF–LII and LII histograms quantifies the relative spatial extents of the PAH and soot containing regions.

References

Arnold A; Becker H; Suntz R; Monkhouse P; Wolfrum J; Maly R; Pfister W (1990) Flame front imaging in an internal-combustion engine simulator by laser-induced fluorescence of acetaldehyde. Opt Lett 15: 831–833

Bengtsson PE; Alden M (1991) C_2 production and excitation in sooting flames using visible laser radiation: implications for diagnostics in sooting flames. Combust Sci Technol 77: 307–318

Bengtsson PE; Alden M (1995) Soot-visualization strategies using laser techniques. Appl Phys 60: 51–59

Beretta F; D'Alessio A; D'Orsi A; Minutolo P (1992) U.V. and visible laser excited fluorescence from rich premixed and diffusion flames. Combust Sci Technol 85: 455–470

Chen LD; Roquemore WM (1986) Visualization of jet flames. Combust Flame 66: 81–86

Coppale A; Joyeux D (1994) Temperature and soot volume fraction in turbulent diffusion flames; measurements of mean and fluctuating values. Combust Flame 96: 275–285

Cignoli F; Benecchi S; Zizak G (1994) Time-delayed detection of laser-induced incandescence for the two-dimensional visualization of soot in flames. Appl Opt 33: 5778–5782

Dasch CJ; Heffelfinger DM (1991) Planar imaging of soot formation in turbulent ethylene diffusion flames; flucturations and integral scales. Combust Flame 85: 389–402

Eckbreth AC; Anderson TJ; Dobbs GM (1986) Conditional sampling for fuel and soot in CARS thermometry. Twenty-First Symposium (International) on Combustion, The Combustion Institute, Pittsburgh, PA pp 1747–1754

Eckbreth AC (1988) Laser diagnostics for combustion temperature and species (A.K. Gupta and D.G. Lilley eds.) Abacus Press, Cambridge MA

Gomez A; Littman MG; Glassman I (1987) Comparative study of soot formation on the centerline of axisymmetric laminar diffusion flames: fuel and temperature effects. Combust Flame 70: 225–241

Hofeldt DL (1993) Real-time soot concentration measurement technique for engine exhaust streams. SAE Tech Paper 930079 (Society of Automotive Engineers) Warrendale, PA

Lockwood FW; Odidi AO (1975) Measurement of mean and fluctating temperature and ion concentration in round turbulent diffusion and premixed flames. Fifteenth Symp (Int) on Combustion, The Combustion Institute, Pittsburgh PA pp 561–563

Longwell JP (1982) The formation of polycyclic aromatic hydrocarbons by combustion. Nineteenth Symposium (International) on Combustion, The Combustion Institute, Pittsburgh PA pp 1339–1350

Lozano A; Yip B; Hanson RK (1992) Acetone: a tracer for concentration measurements in gaseous flows by planar laser-induced fluorescence. Exp Fluids 13: 369–376

Lysaght AJR; Bilger RW; Kent JH (1982) Visualization of mixing in turbulent diffusion flames. Combust Flame 46: 105–108

Melton LA (1984) Soot diagnostics based on laser heating. Appl Opt 23: 2201–2208

Miake-Lye RC; Toner SJ (1987) Laser soot-scattering imaging of a large buoyant diffusion flame. Combust Flame 67: 9–26

Ni T; Pinson JA; Gupta S; Santoro RJ (1995) Two-dimensional imaging of soot volume fraction by the use of laser-induced incandescence. Appl Opt 34: 7083–7091

Nishida O; Mukohara S (1982) Characteristics of soot formation and decomposition in turbulent diffusion flames. Combust Flame 47: 269–279

Nyden MR; Vallikul P; Sivanthanu YR (1996) Tomographic reconstruction of the moments of local probability density functions in turbulent flow fields. J Quant Spectrosc Radiat Transfer 55: 345–356

Prado GP; Lee ML; Hites RA; Hoult DP; Howard JB (1976) Soot and hydrocarbon formation in a turbulent diffusion flame. Sixteenth Symp (Int) on Combustion, The Combustion Institute, Pittsburgh, PA pp 649–659

Quay B; Lee TW; Ni T; Santoro RJ (1994) Spatially resolved measurements of soot volume fraction using laser-induced incandescence. Combust Flame 97: 394–402

Shaddix CE; Harrington JE; Smyth KC (1995) Quantitative Measurements of Enhanced Soot Production in a Flickering Methane/Air Flame. Combust Flame 99: 723–732

Suntz R; Achammer G; Monkhouse P; Schneider M; Kleinermanns K; Wolfrum J (1991) Temperature and pressure dependence of acetaldehyde LIF following excitation at 308 nm. Chem Phys Lett 240: 320–326

Stein SE; Fahr AJ (1985) The high temperature stability of hydrocarbons. J Phys Chem 89: 3714–3725

Tait NP; Greenhalgh DA (1994) 2D Laser induced fluorescence imaging of parent fuel fraction in nonpremixed combustion. Twenty-Fourth Symp (Combustion), The Combustion Institute, Pittsburgh PA pp 1621–1628

Smyth KC; Miller JH; Dorfman RC; Mallard WG; Santoro RJ (1985) Soot inception in a methane/air diffusion flame as characterized by detailed species profiles. Combust Flame 62: 157–181

Turns SR; Lovett JA; Sommer III, HJ (1989) Visualization of soot zones in turbulent diffusion flames. Combust Flame 77: 405–409

Young KJ; Moss JB (1995) Modelling sooting turbulent jet flames using an extended flamelet technique. Combust Sci Technol 105: 33–53

Vander Wal RL; Weiland KJ (1994) Laser-induced incandescence: development and characterization towards a measurement of soot volume fraction. J Appl Phys 59: 445–452

Vander Wal RL; Dietrich DL (1995) Laser-induced incandescence applied to droplet combustion. Appl Opt 34: 1103–1107

Vander Wal RL; Zhou Z; Choi MY (1996a) Laser-induced incandescence calibration via gravimetric sampling. Combust Flame 105: 462–470

Vander Wal RL; Jensen KA; Choi MY (1996b) Simultaneous laser-induced emission of soto and polycyclic aromatic hydrocarbons within a gas-jet diffusion flame. Combust Flame (in press)

Vander Wal RL (1996a) Laser-induced incandescence: Detection Issues. Appl Opt 35: 6548–6559

Vander Wal RL (1996b) Identification of soot precursor material via simultaneous LIF–LII and Characterization via TEM. Combust Sci Technol 118: 343–360

Vander Wal RL (1996c) Soot precursor material: visualization via simultaneous LIF–LII and characterization via TEM. Twenty-Sixth Symp (Int) on Combustion, The Combustion Institute, Pittsburgh, PA (in press)

Wendt JO (1994) Combustion Science for Incineration Technology. Twenty-Fifth Symp (Int) on Combustion, The Combustion Institute, Pittsburgh, PA pp 277–289